Spatially-resolved measurement of electrochemical activity and pH distributions in corrosion processes by scanning electrochemical microscopy using antimony microelectrode tips

Javier Izquierdo[a], Lívia Nagy[c], Ágnes Varga[c], Juan J. Santana[a,b], Géza Nagy[c], Ricardo M. Souto[a,d]

[a] *Department of Physical Chemistry, University of La Laguna, E-38200 La Laguna, Tenerife, Canary Islands, Spain*

[b] *Department of Process Engineering, University of Las Palmas de Gran Canaria, E-35017 Las Palmas de Gran Canaria, Canary Islands, Spain*

[c] *Department of General and Physical Chemistry, Faculty of Sciences, University of Pécs, 7624 Pécs, Ifjúság útja 6, Hungary*

[d] *Instituto Universitario de Materiales y Nanotecnologías, University of La Laguna, E-38200 La Laguna, Tenerife, Canary Islands, Spain*

Abstract

A new method for the spatially-resolved measurement of pH during corrosion processes with the scanning electrochemical microscope (SECM) is presented. Antimony tips are employed because the dual-function characteristics of this material allow the combined amperometric/potentiometric operation of the SECM. The applicability of this technique is illustrated by considering the galvanic corrosion of a model zinc-iron pair immersed in 0.1 M NaCl aqueous solution. Spatially resolved images of pH and oxygen concentration above the metal specimens could be obtained in the same experiment.

Keywords: Scanning electrochemical microscopy; galvanic corrosion; pH distribution; antimony microelectrode.

1. Introduction

Local microcells are formed during the spontaneous corrosion of metals exposed to aqueous environments. That is, spatial distributions of anodes and cathodes on the metallic surface are developed when the material is left at its open circuit potential. The metal is oxidized at the anodes, whereas the corrosion process is maintained by the reduction of some species from the environment at the cathodes (for instance, oxygen in neutral and moderately alkaline media, or protons in acidic solutions). Because the corroding metal usually produces M^{z+} cations transferred under diffusion control at the anodic sites, the system can be studied by SECM [1-3]. This fact has been exploited to image metastable pits on austenitic steel in situ by SECM at the open-circuit potential [4], and to detect metal dissolution either from inclusions in alloys [5-7] or from defects in polymer-coated metals [8-10]. On the other hand, in a neutral aqueous environment, oxygen from the electrolyte is consumed at the cathodic areas, and the reaction may be detected by the scanning tip as local depletion of the oxygen concentration in the electrolyte adjacent to cathodic sites [11-15]. These studies have gathered new spatially-resolved information on the mechanisms of localized corrosion reactions in overwhelming cases employing metal microdisks as the tip and the amperometric operation of the SECM. That is, the electrochemical information is obtained from the measurement of the faradaic current flowing in the ultramicroelectrode tip as a function of either time or its location above the sample.

Corrosion processes are very sensitive to pH, and the progress of the corrosion reactions may produce changes in the pH of the environment too. Cathodic half-cell reactions often involve a progressive alkalinisation of the electrolyte, either by consuming protons if the electrolyte is originally acidic, or by releasing hydroxyl ions in the case of neutral or alkaline solutions. Additionally, the corrosion of the metal at the anodic sites results in the generation of metal ions, and some of them undergo hydrolysis reactions with the aqueous environment, producing local acidification of the medium. Thus, the measurement of pH in the vicinity of a corroding surface and its visualization as a function of the location at the surface, and its evolution with time are of major interest to a better understanding of the corrosion processes in micrometric and submicrometric scales.

Though pH imaging is possible by using SECM in potentiometric operation since an antimony tip was developed for ion-selective potentiometric microscopy in 1993 [16], this method has not been applied in Corrosion Science yet. The electric potential of this material changes in response to variations in the acidity of the environment due to its tendency to be coated by a Sb_2O_3 film. Thus, antimony tips have been employed as pH sensor in SECM for the characterization of a variety of systems [17-19], as well as microsensors for other techniques [20-28]. Due to the metallic

properties of antimony, tips from this material can also be employed in amperometric SECM to image the topography of the substrates under investigation [16,18], thus allowing more information to be gained from these systems. That is, antimony tips are dual-function microelectrodes applicable for both amperometric and potentiometric SECM. This is a major advantage compared to other ISMEs employed for pH monitoring in SECM which can only be employed for the potentiometric operation [29-34] or with the scanning ion-selective electrode technique (SIET) [35,36]. This dual-function property has application not only for SECM, because it has been employed for the detection of heavy metals with square-wave voltammetry when carbon-based microelectrodes were coated with antimony thin films [37-39].

In this work we are reporting preliminary results obtained from SECM measurements with an antimony tip to characterize a model corrosion reaction. The experimental system selected for this work was the galvanic corrosion of a zinc-iron pair, an experimental system previously characterized by amperometric SECM [12], scanning vibrating electrode technique (SVET) [12,40], and SIET [36]. The dual function of the tip material was explored for the combined potentiometric monitoring of pH distributions and the amperometric detection of dissolved oxygen employed as redox mediator [13].

2. Experimental

Antimony microelectrodes were made of two parts as shown in **Figure 1**. The outer glass capillary provides the electric connection, whereas the actual antimony tip is inserted into the lumen of the first. High purity antimony in powder presentation (266329, Aldrich) and borosilicate glass capillaries (B200-116-10, Sutter Instruments, Novato, CA, USA) were used.

The fabrication of the microelectrode is initiated by heating the antimony powder in a melting pot with the help of a gas flame. When antimony melts, one glass capillary is filled with it using syringe suction. The filled capillary is then pulled using metallic tweezers to produce a smaller size glass capillary filled with antimony. Further pulling with a micropipette puller (mod. P-30/P, Sutter) allowed one section of this conic tip, with an approximate diameter of 15 – 20 μm, to be fabricated. A second glass capillary was also pulled to produce at its end a capillary of dia. 100 μm, and the antimony tip was next inserted in its lumen with the tip reaching out for about 15 mm, and about 20 mm long staying in the lumen. Mercury metal and the copper wire were then inserted into the lumen of the thicker capillary to provide electrical contact. Loctite adhesive was used to seal both ends.

In this work, we investigated the corrosion behaviour of a zinc-iron galvanic pair. The samples were prepared from high purity strips of each metal supplied as sheets by Goodfellow Materials Ltd. (Cambridge, UK), with nominal purities of 99.5% for iron and 99% for zinc. The metals were cut into 1x1 mm^2 strips, and mounted in an Epofix epoxy sleeve (Struers, Ballerup, Denmark)

with a separation of ca. 1 mm between them. The mounts with the samples were polished with silicon carbide paper down to 800 grit, and subsequently polished with alumina micropolish of 1 and of 0.3 μm particle size. The resulting surfaces were thoroughly rinsed with Millipore deionised water, dried with acetone and finally surrounded laterally by sellotape, thus creating a small container for the test electrolyte solution. The two metals were electrically connected at the back of the epoxy mount to form a galvanic couple. The electrochemical cell was completed with an Ag/AgCl, 3M KCl reference electrode, and a platinum wire as the counter electrode.

A home-built SECM system was employed [17], using a 3D positioning device driven by precision step motors with 75 nm minimal step size. A video camera was used to further assist positioning of the tip close to the surface. The distance between the tip and the substrate was established by allowing the probe to gently rest on the sample, and subsequently the probe was retreated to the chosen operation distance with the aid of the *Z*-positioning motor. Tip-surface distance was also estimated using the negative feedback function measured for the oxygen reduction current when the tip was located over the epoxy part. Selected experiments were also performed using a platinum microelectrode of 25 μm diameter to check the effect of the metal used to build the tip in amperometric SECM.

Reagents of analytical grade and bidistilled water were employed to prepare all the solutions. The pH calibration of the antimony microelectrodes was made in the buffer solutions listed in **Table 1**. They were prepared from 0.1 M solutions of the basic species, and the pH was adjusted by adding HCl. Corrosion tests were carried out in aqueous 0.1 M NaCl solution.

3. Results and discussion

3.1. Calibration of the antimony microelectrode

Antimony microelectrodes were calibrated by measuring their open circuit potentials in the buffer solutions given in Table 1. The typical calibration procedure was performed by introducing the microelectrode in a sequence of buffer solutions initiated with the most alkaline solution. In this way, the tip was exposed to solutions of increased acidity as shown in **Figure 2.** The overpotential values observed in the plot occurred upon electrolyte exchange, and next the electrode attained a steady potential value in each solution. No steady value of the electrode potential could be observed when it was introduced in the buffer solution of pH 3.07, because the antimony electrode was not stable in this medium due to acid attack. In this medium, the initial potential value in the transient was taken for calibration purposes. Finally, the electrode was reintroduced in the most alkaline buffer solution to check the reproducibility of its potential response. The potential value measured after a quite short stabilization period was the same as that recorded at the beginning of the experiment within

experimental error of 1.5 mV. With the potential values taken from each buffer solution, the calibration plot shown in the inset of the figure was drawn. It can be observed that there is a linear relationship between the potential of the antimony tip and the solution pH in the interval between 3 and 11.5. The slope of the plot amounts 46.1 mV/pH unit.

3.2. SECM visualization of pH and oxygen concentration distributions during the galvanic corrosion of a zinc-iron pair

The dual function of the antimony microelectrode used as tip in scanning electrochemical microscopy was explored on a zinc-iron galvanic pair immersed in naturally aerated 0.1 M NaCl solution at ambient temperature. The tip-substrate distance was established by allowing the antimony tip to gently rest on the surface of the epoxy sleeve half way between the two metals. After the tip was retreated to a height of 25 µm, SECM scan lines or arrays were registered above the zinc specimen by scanning the tip parallel to the surface.

Figure 3 displays the pH values measured with the antimony tip operated in potentiometric mode while scanning a line passing above the centre of the two metals after they have been immersed in the test solution for about 120 min. Alkalinisation of the electrolyte occurred in the proximity of the iron sample, which is the nobler metal in the galvanic pair. Thus, the cathodic process takes place on this metal. In an acidic electrolyte, protons are removed from the electrolyte as they are electroreduced to hydrogen at the cathodic sites:

$$2H^+ + 2e^- \rightarrow H_2(g) \qquad (1)$$

whereas in neutral and alkaline environments, the electroreduction of dissolved oxygen releases hydroxide ions into the solution according to:

$$O_2 + 4H_2O + 4e^- \rightarrow 4OH^- \qquad (2)$$

Since the initial electrolyte is slightly acidic, equation (1) could be considered to occur first on the surface of iron, followed by the electroreduction of oxygen at a later stage. Yet, the simultaneous occurrence of oxygen electroreduction can be checked by using the antimony microelectrode as conventional tip in amperometric SECM. In this case, the potential of the tip was set at -0.65 V vs. (Ag/AgCl, 3M KCl) to detect the concentration distribution of dissolved oxygen above the iron sample. The same feature is clearly observed when the current value normalized to the bulk current (I/I_{lim}) during a scan line taken over the centre of the image, was determined with the antimony microelectrode (see **Figure 4A**). In the later, the *Y* axis has been inversed to show smaller cathodic

faradaic currents to fall lower in the graph, thus effectively corresponding to lower oxygen contents. In order to check the validity of this method, a platinum tip was also employed. The scan array given in **Figure 4B** displays a region of depleted oxygen concentration extending over the dimensions of the iron sample as recorded with the platinum microelectrode. In summary, oxygen is consumed at the cathodic sites through equation (2) at a higher rate than diffusion can supply it from the bulk of the electrolyte. Thus, the consumption of oxygen can be monitored by amperometric SECM with antimony tips as they provide the same results than conventional platinum microelectrodes.

The alkalinisation process continues with the elapse of time for the duration of the experiment, and even higher pH values are measured after 26 hours immersion of the galvanic pair in the electrolyte. The distribution of pH from the surface towards the bulk of the electrolyte can be obtained simply by stepwise changing the tip-sample distance during the measurements. This procedure is illustrated in **Figure 5A** which corresponds to the tip positioned directly above the center of the iron specimen. The tip was first removed from the vicinity of the surface to a distance of 900 μm, and then the direction of the tip movement was reversed for the probe to approach the surface again. The pH drops by almost 4 units during the retreating movement from the iron surface, whereas a stationary value is observed in the approach scan for distances in excess of 400 μm. This pH value corresponds to the bulk electrolyte after the galvanic corrosion process has proceeded for 26 hours. At shorter distances, a fast increase of pH values is observed as the tip continues approaching the iron surface until the initial value on the proximity of the metal is measured again. The two pH-distance curves obtained during retreat and subsequent approach of the tip to the surface thus describe a hysteresis loop. The origin of this feature can be attributed to the movement of the electrolyte that produces convective effects in the electrolyte. The slower decay of pH from the surface to the bulk electrolyte during the retreating movement happens because the tip leaves a hydroxide-rich region that constitutes the confined electrolyte volume formed between the tip and the iron surface for the previous 26 hours, and thus its movement is accompanied by a portion of this electrolyte that dilutes slower than the tip moves from the surface. This effect is less pronounced during the approach movement as the tip moves from a volume with very small concentration of hydroxide ions to much richer concentrations. The response time of most sensors is smaller in direction of concentration increase than in the opposite direction. The dilution effects due to tip movement are below the detection limit of the experimental technique in this case.

The spatial distribution of pH can be imaged when scan arrays are measured instead. They can be recorded either in a plane parallel to the surface, the arrays effectively being a composition of scan lines as that constituting Figure 3, or in a plane perpendicular to the surface. In the later case, the distribution of pH from the surface into the electrolyte is imaged instead. **Figure 6** shows the pH distribution obtained above the iron sample. The map is composed by scan lines registered

at different distances from the surface. Since the distance covered in each scan line is rather long to allow the pH distribution to be appreciated over a large area of the system, rather long acquisition times were required to measure each scan line, and they were registered only at some selected heights. Yet the spatial distribution of pH values from the surface into the bulk electrolyte can be clearly observed from the inspection of this image.

The pH distribution over the zinc sample was also investigated. The pH distribution over this metal looks almost homogeneous from the observation of the scan arrays, even for the longest exposures as shown in **Figure 7**. Nevertheless, some distribution of pH values occurs above the zinc sample when the data are plotted with greater resolution (cf. inset in Figure 3). Thus, some acidification happens in this case, though the magnitude of this effect is significantly smaller than the alkalinisation process occurring at the cathode. Furthermore, the pH distribution over the metal remains quite homogeneous over its whole surface. It is concluded that metal dissolution occurs at the surface of the zinc specimen according to reaction:

$$Zn \rightarrow Zn^{2+} + 2e^{-} \qquad (3)$$

The dissolution process does not produce a variation in the pH of the electrolyte as given by equation (3), unless a certain amount of the released metal ions undergo hydrolysis in the electrolyte as given by:

$$Zn^{2+} + nH_2O \rightarrow Zn(OH)_n^{2-n} + nH^{+} \qquad (4)$$

In this case, local acidification of the electrolyte would happen in the proximity of the zinc electrode.

Though the bulk electrolyte becomes progressively more alkaline with the elapse of time as shown above, the zinc surface remains slightly more acidic than the bulk even after 27 hours. This fact can be easily observed from the retreat and subsequent approach plots shown in **Figure 5B,** which were measured with the tip located above the centre of the zinc specimen. The small concentration variations occurring in this case are not significantly affected by the mechanical movement of the tip, and both plots lie very close to each other.

4. Conclusions

The use of an antimony microelectrode as tip in a scanning electrochemical microscope greatly enhances the information gathered on corrosion reactions by allowing the spatial distribution of pH to be imaged (quasi) simultaneously to the conventional amperometric operation of the instrument

in the generation-collection mode. This new methodology can be used to investigate a wide variety of corrosion systems, though its most immediate application can be found in the characterization of the sacrificial protection imparted by zinc to iron-base alloys in general, and to galvanized steels in particular.

Acknowledgements:

The authors are grateful to the National Office for Research and Technology (NKTH, Budapest, research grant ES-25/2008 TeT) and to the Spanish Ministry of Science and Innovation (MICINN, Madrid, Acción Integrada No. HH2008-0011) for the grant of a Collaborative Research Programme between Hungary and Spain. J.I. and R.M.S. are grateful for financial support by the MICINN and the European Regional Development Fund (Brussels, Belgium) under Project No. CTQ2009-12459. A Research Training Grant awarded to JI by the MICINN (*Programa de Formación de Personal Investigador*) is gratefully acknowledged.

References:

1. S.E. Pust, W. Maier, G. Wittstock, Investigation of localized catalytic and electrocatalytic processes and corrosion reactions with scanning electrochemical microscopy (SECM), Z. Phys. Chem. 222 (2008) 1463–1517.
2. L. Niu, Y. Yin, W. Guo, M. Lu, R. Qin, S. Chen, Application of scanning electrochemical microscope in the study of corrosion of metals, J. Mater. Sci. 44 (2009) 4511–4521.
3. R.M. Souto, S. Lamaka, S. González, Uses of scanning electrochemical microscopy in corrosion research, in: A. Méndez-Vilas, J. Díaz (Eds.), Microscopy: Science, technology, applications and education, Vol. 3; Formatex Research Center, Badajoz (Spain), 2010, pp. 2162-2173.
4. Y. González-García, G.T. Burstein, S. González, R.M. Souto, Imaging metastable pits on austenitic stainless steel *in situ* at the open-circuit corrosion potential, Electrochem. Commun. 6 (2004) 637-642.
5. C.H. Paik, H.S. White, R.C. Alkire, Scanning electrochemical microscopy detection of dissolved sulfur species from inclusions in stainless steel, J. Electrochem. Soc. 147 (2000) 4120-4124.
6. C.H. Paik, R.C. Alkire, Role of sulfide inclusions on localized corrosion of Ni200 in NaCl solutions, J. Electrochem. Soc. 148 (2001) B276-B281.
7. K. Fushimi, M. Seo, An SECM observation of dissolution distribution of ferrous or ferric ion from a polycrystalline iron electrode, Electrochim. Acta 47 (2001) 121-127.

8. R.M. Souto, Y. González-García, S. González, *In Situ* monitoring of electroactive species by using the scanning electrochemical microscope. Application to the investigation of degradation processes at defective coated metals, Corros. Sci. 47 (2005) 3312-3323.
9. A.M. Simoes, D. Battocchi, D.E. Tallman, G.P. Bierwagen, SVET and SECM imaging of cathodic protection of aluminium by a Mg-rich coating, Corros. Sci. 49 (2007) 3838-3849.
10. S. González, J.J. Santana, Y. González-García, L. Fernández-Mérida, R.M. Souto, Scanning electrochemical microscopy for the investigation of localized degradation processes in coated metals: Effect of oxygen. Corros. Sci. 53 (2011) 1910-1915.
11. A.C. Bastos, A.M. Simões, S. González, Y. González-García, R.M. Souto, Imaging concentration profiles of redox-active species in open-circuit corrosion processes with the scanning electrochemical microscope, Electrochem. Commun. 6 (2004) 1212-1215.
12. A.M. Simões, A.C. Bastos, M.G. Ferreira, Y. González-García, S. González, R.M. Souto, Use of SVET and SECM to study the galvanic corrosion of an iron-zinc cell, Corros. Sci. 49 (2007) 726-739.
13. R.M. Souto, L. Fernández-Mérida, S. González, SECM imaging of interfacial processes in defective organic coatings applied on metallic substrates using oxygen as redox mediator, Electroanalysis 21 (2009) 2640-2646.
14. J.J. Santana, J. González-Guzmán, L. Fernández-Mérida, S. González, R.M. Souto, Visualization of local degradation processes in coated metals by means of scanning electrochemical microscopy in the redox competition mode, Electrochim. Acta 55 (2010) 4488-4494.
15. Y. Gonzalez-Garcia, J.M.C Mol, T. Muselle, I. De Graeve, G. Van Assche, G. Scheltjens, B. Van Mele, H. Terryn, SECM study of defect repair in self-healing polymer coatings on metals, Electrochem. Commun. 13 (2011) 169-173.
16. B. Horrocks, M.V. Mirkin, D.T. Pierce, A.J. Bard, G. Nagy, K. Toth, Scanning electrochemical microscopy. 19. Ion-selective potentiometric microscopy. Anal. Chem. 65 (1993) 1213-1224.
17. B. Kovács, B. Csóka, G. Nagy, I. Kapui, R.E. Gyurcsányi, K. Tóth, Automatic target location strategy - A novel approach in scanning electrochemical microscopy, Electroanalysis 11 (1999) 349-355.
18. B. Liu, W. Cheng, S.A. Rotenberg, M.V. Mirkin, Scanning electrochemical microscopy of living cells: Part 2. Imaging redox and acid/basic reactivities, J. Electroanal. Chem. 500 (2001) 590-597.
19. B. Csóka, B. Kovács, G. Nagy, Investigation of concentration profiles inside operating biocatalytic sensors with scanning electrochemical microscopy (SECM), Biosens. Bioelectronics 18 (2003) 141-149.

20. T. Honda, K. Murase, T. Hirato, Y. Awakura, pH measurement in the vicinity of a cathode evolving hydrogen gas using an antimony microelectrode, J. Appl. Electrochem. 28 (1998) 617-622.
21. F.L. Rosenfeldt, R. Ou, J.A. Smith, D.E. Mulcahy, J.T. Bannigan, M.R. Haskard, Evaluation of a miniature antimony electrode for measurement of myocardial pH, J. Med. Eng. Technol. 23 (1999) 119-126.
22. A.N. Ivanov, G.A. Evtugyn, R.E. Gyurcsányi, K. Tóth, H.C. Budnikov, Comparative investigation of electrochemical cholinesterase biosensors for pesticide determination, Anal. Chim. Acta 404 (2000) 55-65.
23. F. Sjöberg, G. Nilsson, Dual mode antimony electrode for simultaneous measurements of pO_2 and pH, Acta Anesthesiol. Scand. 44 (2000) 32-36.
24. Y. Tsuru, M. Nomura, F.R. Foulkes, Effects of boric acid on hydrogen evolution and internal stress in films deposited from a nickel sulfamate bath, J. Appl. Electrochem. 32 (2002) 629-634.
25. Y. Ha, M. Wang, Capillary melt method for micro antimony oxide pH electrode, Electroanalysis 18 (2006) 1121-1125.
26. M. Wang, Y. Ha, An electrochemical approach to monitor pH change in agar media during plant tissue culture, Biosens. Bioelectronics 22 (2007) 2718-2723.
27. A. Avdić, A. Lugstein, C. Schöndorfer, E. Bertagnolli, Focused ion beam generated antimony nanowires for microscale pH sensors, Appl. Phys. Lett. 95 (2009) 223106-1-3.
28. W. Vonau, W. Oelßner, U. Guth, J. Henze, An all-solid-state reference electrode, Sens. Actuators B 144 (2010) 368-373.
29. N. Radić, H.B. Mark Jr., A polymeric sulfur nitride, $(SN)_x$, electrode responsive to pH and its application to the aqueous potentiometric titration of weak acids, Anal. Chim. Acta 144 (1982) 253-259.
30. P.J. Kinlen, J.E. Heider, D.E. Hubbard, A solid-state pH sensor based on a Nafion-coated iridium oxide indicator electrode and a polymer-based silver chloride reference electrode, Sens. Actuators B 22 (1994) 13-25.
31. R.E.F. Einerhand, W.H.M. Visscher, E. Barendrecht, pH measurement in strong KOH solutions with a bismuth electrode, Electrochim. Acta 34 (1989) 345-353.
32. L.J. Bloor, D.J. Malcolme-Lawes, An electrochemical preparation of palladium oxide pH sensors, J. Electroanal. Chem. 278 (1990) 161-173.
33. M.J. Tarlov, S. Semancik, K.G. Kreider, Mechanistic and response studies of iridium oxide pH sensors, Sens. Actuators B 1 (1990) 293-297.

34. K. Yamamoto, G. Shi, T. Zhou, F. Xu, M. Zhu, M. Liu, T. Kato, J.-Y. Jin, L. Jin, Solid-state pH ultramicrosensor based on a tungstic oxide film fabricated on a tungsten nanoelectrode and its application to the study of endothelial cells, Anal. Chim. Acta 480 (2003) 109-117.
35. M.F. Montemor, W. Trabelsi, S.V. Lamaka, K.A. Yasakau, M.L. Zheludkevich, A.C. Bastos, M.G.S. Ferreira, The synergistic combination of bis-silane and $CeO_2 \cdot ZrO_2$ nanoparticles on the electrochemical behaviour of galvanised steel in NaCl solutions, Electrochim. Acta 53 (2008) 5913-5922.
36. S.V. Lamaka, M. Taryba, M.F. Montemor, H.S. Isaacs, M.G.S. Ferreira, Quasi-simultaneous measurements of ionic currents by vibrating probe and pH distribution by ion-selective microelectrode, Electrochem. Comm. 13 (2011) 20-23.
37. E. Tesarova, L. Baldrianova, S.B. Hocevar, I. Svancara, K. Vytras, B. Ogorevc, Anodic stripping voltammetric measurement of trace heavy metals at antimony film carbon paste electrode, Electrochim. Acta 54 (2009) 1506-1510.
38. V. Guzsvany, H. Nakajima, N. Soh, K. Nakano, T. Imato, Antimony-film electrode for the determination of trace metals by sequential-injection analysis/anodic stripping voltammetry, Anal. Chim. Acta 658 (2010) 12-17.
39. H. Sopha, L. Baldrianova, E. Tesarova, S.B. Hocevar, I. Svancara, B. Ogorevc, K. Vytras, Insights into the simultaneous chronopotentiometric stripping measurement of indium(III), thallium(I) and zinc(II) in acidic medium at the in situ prepared antimony film carbon paste electrode, Electrochim. Acta 55 (2010) 7929-7933.
40. R.M. Souto, Y. González-García, A.C. Bastos, A.M. Simões, Investigating corrosion processes in the micrometric range: A SVET study of the galvanic corrosion of zinc coupled with iron, Corros. Sci. 49 (2007) 4568-4580.

Table 1. Buffer solutions employed for the calibration of the antimony microelectrode.

pH value	Buffer System
11.50	HPO_4^{2-} / PO_4^{3-}
10.34	HCO_3^- / CO_3^{2-}
8.23	NH_4^+ / NH_4OH
7.45	$H_2PO_4^-$ / HPO_4^{2-}
6.36	$H_2PO_4^-$ / HPO_4^{2-}
4.50	$H_3C_2O_2H$ / $H_3C_2O_2^-$
3.07	H_3PO_4 / $H_2PO_4^-$

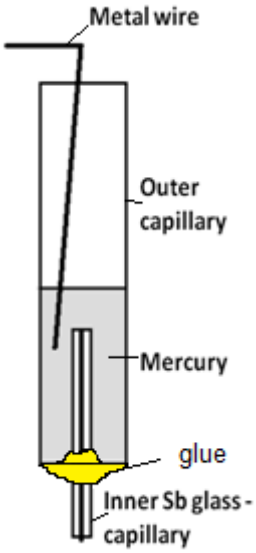

Figure 1

Sketch of the antimony microelectrode.

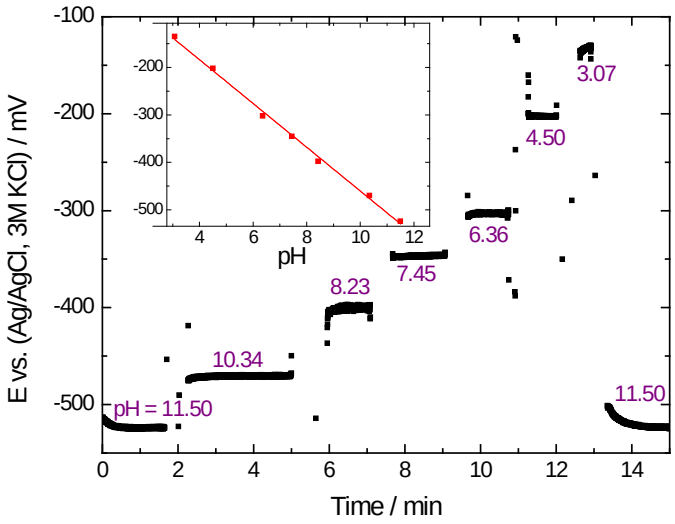

Figure 2

Dynamic response transients of the antimony microelectrode to pH. The pH changes were made by replacing the buffer solutions described in Table 1. The inset depicts the resulting calibration plot.

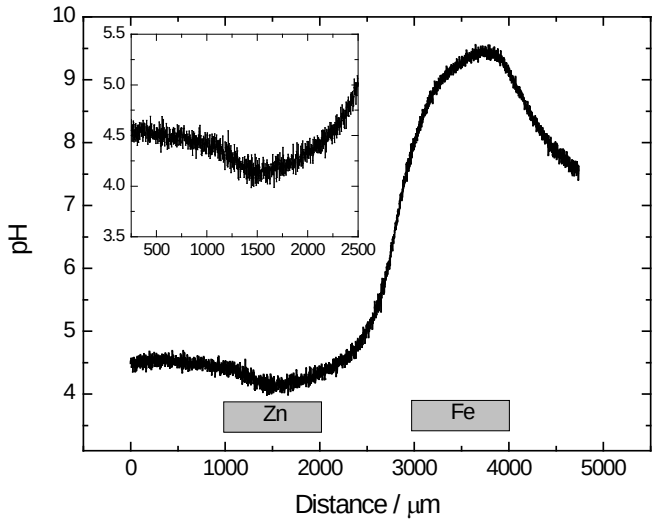

Figure 3

Potentiometric scan line of the antimony probe tip above the zinc-iron galvanic couple after 3 hours immersion in 0.1 M NaCl. The inset shows the pH variation measured above the zinc sample with greater resolution. Tip-sample distance: 25 µm; scan rate: 5 µm/s.

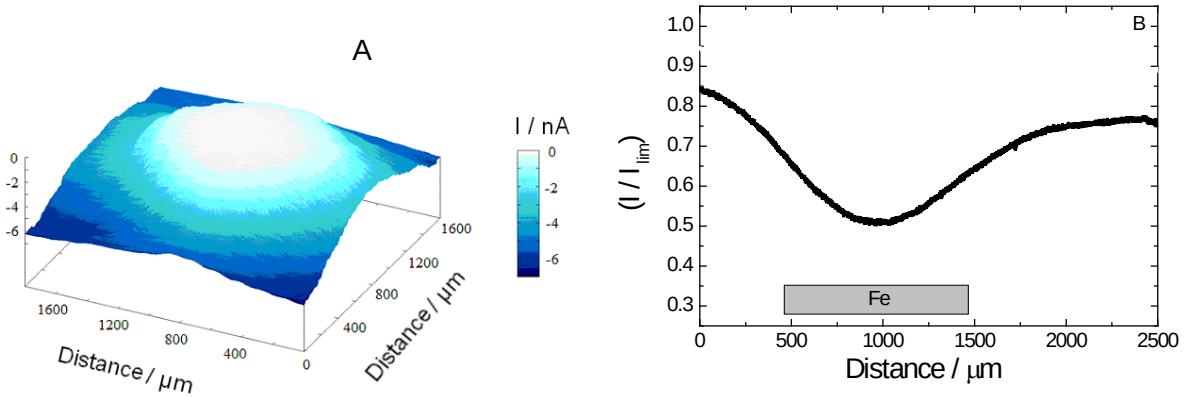

Figure 4

Distribution of oxygen concentration above the iron sample immersed in 0.1 M NaCl for 7 hours. SECM operating amperometrically by setting the tip potential at -0.65 V vs. (Ag/AgCl, 3M KCl). Tip-sample distance: 25 µm. (A) SECM map depicting the absolute current measured at a platinum microelectrode; scan rate: 30 µm/s. (B) scan line depicting the normalized current (I/I_{lim}) for a trip of the antimony tip along *X* axis passing over the centre of the sample; scan rate: 5 µm/s.

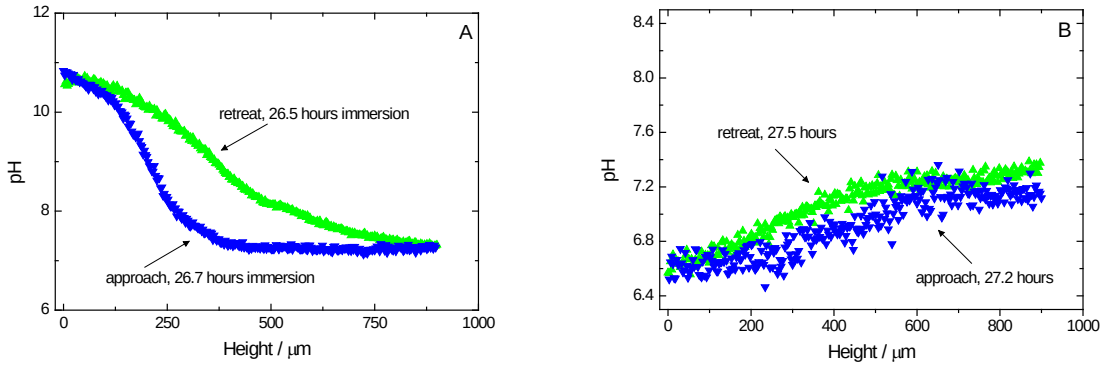

Figure 5

pH distributions above (A) iron and (B) zinc specimens measured with the antimony tip as the height of the tip is changed relative to the surface. The zinc-iron galvanic pair has been immersed in 0.1 M NaCl for the immersion times given in the graphs.

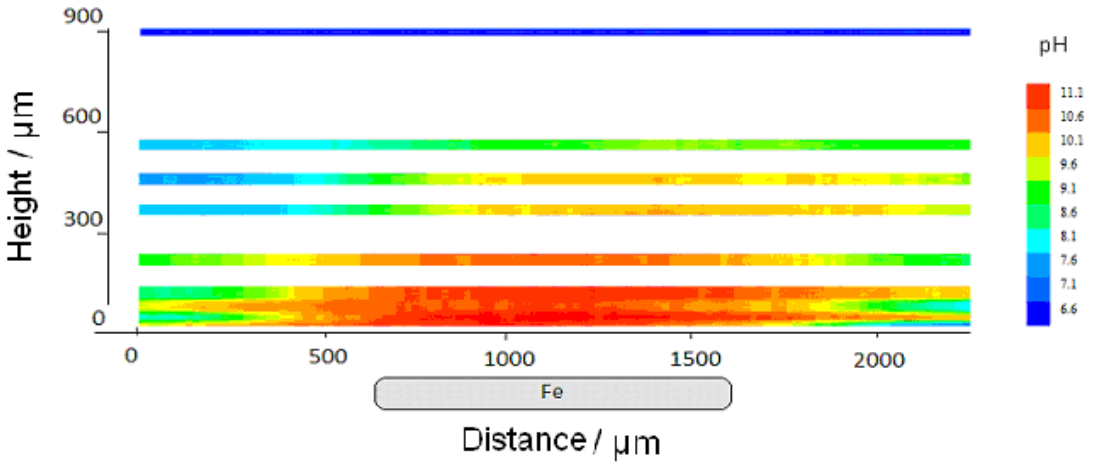

Figure 6

pH distribution in a plane perpendicular to the surface of the iron specimen 22 hours registered after the iron-zinc pair has been immersed in 0.1 M NaCl during. Lateral scanning rate 5 µm/s. In order to shorten experimental time only 8 lateral scans at different distances were performed.

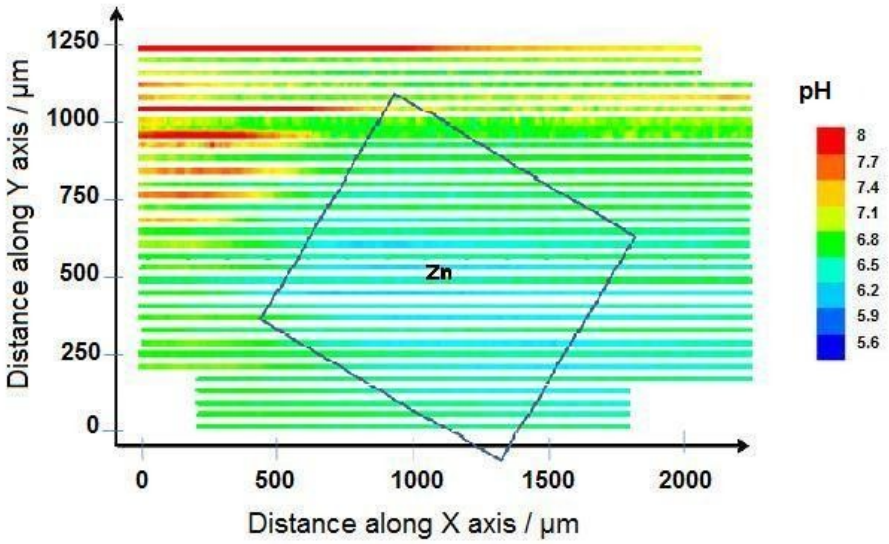

Figure 7

pH distribution in a plane parallel to the surface of the zinc specimen after the iron-zinc pair has been immersed in 0.1 M NaCl during 7 hours.